Numerical and experimental modelling of back stream flow during close-coupled gas atomization

Shahed Motaman, Andrew M. Mullis, Robert F. Cochrane and Ian N. McCarthy

Institute for Materials Research
University of Leeds, Leeds, UK, LS2 9JT

Duncan J. Borman

School of Civil Engineering
University of Leeds, Leeds, UK, LS2 9JT

Abstract

This paper reports the numerical and experimental investigation into the effects of different gas jet mis-match angles (for an external melt nozzle wall) on the back-stream flow in close coupled gas atomization. The Pulse Laser Imaging (PLI) technique was applied for visualising the back-stream melt flow phenomena with an analogue water atomizer and the associated PLI images compared with numerical results. In the investigation a Convergent–Divergent (C-D) discrete gas jet die at five different atomization gas pressures of 1 to 5 MPa, with different gas exit jet distances of 1.65, 1.6, 1.55, 1.5, 1.45 and 1.40 mm from the melt nozzle external wall, was combined with four melt nozzles of varying gas jet mis-match angles of 0, 3, 5, and 7 degrees relative to the melt nozzle external wall (referred to as nozzle types 1 to 4). The results show that nozzle type 1 with the smallest mis-match angle of zero degrees has highest back-stream flow at an atomization gas pressure of 1 MPa and a gas die exit jet located between 1.65 mm to 1.5 mm from the external melt nozzle wall. This phenomenon decreased with increasing mis-match angle and at higher atomization gas pressure. For nozzle type 2, with a mis-match angle of 3 degrees, a weak back-stream flow occurred with a gas exit jet distance of 1.65 mm from the melt nozzle external wall. For a gas pressure of 1 MPa with a decrease in the gas jet exit distance from the external wall of the melt nozzle this phenomenon was eliminated. This phenomenon was not seen for nozzle types 3 and 4 at any gas pressure and C-D gas exit jet distances.

Key words

Mis- match angle; Back–stream flow; Gas atomization; External wall; Melt nozzle

1. Introduction

Gas atomization is a technique for producing fine spherical powder metals and alloys. There are two general methods for the gas atomization; free fall and close-coupled gas atomization (CCGA). In free fall atomization, the molten metal falls a short distance from the melt delivery nozzle under gravity before being broken apart by an impinging gas jet. A positive aspect of the free fall design is that it is easier to control the gas and melt interaction when compared with a close-coupled design. However, in free fall designs the particle size distribution is difficult to control and the process efficiency is lower. As such, most commercial atomizer tends to be of the close-coupled design. In close coupled atomization, the molten metal stream pours from a tundish that acts as a reservoir controlling the flow rate

of the molten metal into the atomizing chamber (which consists of a melt feed nozzle and gas manifold or die). In this chamber the liquid metal is disrupted by the impact of high velocity jets (typically of air, nitrogen or argon) just below the melt feed nozzle exit tip, forming melt droplets which subsequently solidify to form spherical particles. The selection of gas type is dependent on the metal properties, particularly if oxidation of the melt needs to be avoided, although gas type will also significantly influence the particle cooling rate. In the close couple process the melt ligament can be disrupted more efficiently than in the free-fall process due to the close proximity between gas jets and the melt delivery nozzle. This minimizes the dissipation of energy in the gas and as a result particles of a finer size distribution, requiring reduced energy consumption, are achieved [1, 2].

In close-coupled commercial gas atomizers the geometry of the gas delivery system, which is known as the gas die, is very important. The geometry of features such as exit area, apex angle, jet design (e.g. whether Convergent-Divergent (C-D) or cylindrical in shape and whether of the annular slit or discrete jet gas die configuration) play a crucial role in defining factors that determine how the high velocity gas jet interacts with the molten metal [3]. Oversights in any of above mentioned features can result in unsteady atomization, increasing the production costs or decreasing the efficiency of the process [1,3].

The annular slit design is widely used in commercial atomizers and has been favoured for many years in the gas atomizer industry [3]. The gas die assembly consists of a circular opening fed by a high pressure gas plenum, in the geometrical centre of which is positioned the melt delivery nozzle. The outer surface of the melt nozzle thus acts as the inner surface of the gas outlet manifold. This gas die design has a large exit area and subsequently has higher gas flow rates when compared to the discrete jet design [3,4]. This type of gas die configuration is often used for moderate inlet gas pressure atomizers to prevent excessive gas consumption. It is also much simpler to manufacture compared to the more complex discrete jet gas die [4]. A difficulty with this design type can be the alignment of the melt delivery nozzle within the die. Any axial miss alignment of the gas die with respect to the melt delivery nozzle will result in uneven gas flow and can cause atomization not to take place as intended [3,4].

The idea of using discrete jet gas die systems was motivated by the increasing demand for finer powders, which require higher gas atomization pressures [3,4]. Unlike the annular slit design, the melt delivery nozzle does not form part of the surface confining the gas flow. Instead the gas flow is through a numbers of individual jets drilled into the die around the circumference of the melt delivery nozzle [4,7]. Due to the decrease in exit area of the gas jet a lower gas volume is consumed at the same inlet pressure in comparison with the annular slit design. This leads to improved particle size control and refinement through use of higher gas pressure while maintaining similar gas consumption rates to that of an annular slit designs [3, 4].

The gas jet in the annular slit and discrete jet system can be of either the cylindrical or C-D design. In a cylindrical jet choked flow occurs, with the gas velocity in the jet being restricted to Mach 1. Upon exit the gas expands and accelerates to supersonic velocity. However, due to the uncontrolled expansion, the gas jet spreads out and its momentum is rapidly dissipated limiting the kinetic energy imparted to the melt stream. In contrast, a C-D or de Laval gas jet will accelerate the gas to supersonic velocity in the divergent section of the nozzle, providing a directed high-speed jet of gas. The C-D nozzle's more complex internal shape enables the exiting gas jet to maintain a higher velocity which is favourable for generating good quality powders in the close coupled gas atomizer [4,8,9].

The gas flow is constrained at the minimum cross section of the nozzle a region known as the throat. In this area the gas pressure is a maximum. After the throat the exit area widens, allowing controlled expansion of the gas, wherein its velocity reaches supersonic levels. Based on isentropic theory the ratio of the exit to throat area determines the gas velocity at the exit according to Eq. (1):

$$\frac{A}{A_t} = \left(\frac{1+\gamma}{\gamma}\right)^{-K} \frac{\left(1+\left(\frac{\gamma-1}{2}\right) M^2\right)^K}{M} \qquad (1)$$

Where $K = \frac{\gamma+1}{2(\gamma-1)}$

In the Eq. (1): $\frac{A}{A_t}$ is the ratio of the exit area to throat area , γ is the ratio of specific heat capacities, and M is Mach number. The outlet Mach number also determines the design criteria for the ratio of the inlet pressure and the ambient pressure by Eq. (2):

$$\frac{P}{P_0} = \left(1 + \left(\frac{\gamma-1}{2}\right) M^2\right)^{\frac{\gamma}{\gamma-1}} \qquad (2)$$

Operation of the system at pressures below the design pressure for the C-D gas die leads to over-expanded flow. Conversely, running the a C-D gas die at too high a pressure for the design will causes the gas not to be fully expanded and in which case it will exhibit under-expanded behaviour. Both these gas flow conditions may cause oblique shock waves at the nozzle exit which will decrease the kinetic energy of the gas jet which are not favourable for atomization [3,4].

There are a number of unresolved issues with close-coupled gas atomization due to the complexity of the process and a deficiency of knowledge regarding gas-melt interactions and control parameter which influence the process. However this process is still the most practical method for producing high quality powder metals [3]. One of the problems during the close coupled gas atomization process is back-streaming of the melt, which occurs when the molten metal is drawn back up the outer surface of the melt delivery nozzle, wherein it solidifies as a result of being exposed to very cold expanding gas. This in turn leads to an alteration of the geometry of the melt delivery nozzle as a consequence of which the molten metal may freeze-off causing production to be aborted. Fig. 1 shows a ceramic melt delivery nozzle that has failed during gas atomization of Ni-Al melt [5].

The gas flow separation is an undesirable feature in the close-coupled gas atomization process. Two explanations have been proposed for this problem [10]. One explanation suggests gas flow separation in which the gas boundary layers around the outer surface of the melt delivery nozzle wall separate from the wall surface creating a negative pressure gradient in this region. This negative pressure gradient draws the molten metal into this region. The other mechanism mostly relates to the case of discrete gas die systems is referred to in this work as Discrete Jet Pressure Inversion (DJPI). Both have the same result with the consequence being the melt freeze off problem around the melt delivery nozzle.

However, unlike the flow separation mechanism, which is related to the external geometry of the melt nozzle (specially melt nozzle tip length), the DJPI has a different mechanism and is more likely to occur in a discrete jet gas die system and where the inclined angle of the melt nozzle external wall changes with gas jet die design. This aspect has yet to be fully investigated by researchers. Fig. 2 shows the schematic representation of the flow separation phenomenon and the proposed DJPI mechanism that has been observed in experiments.

Previous numerical investigations concerning the back-stream flow problem around the melt nozzle tip were primarily focused on flow separation and the relation between melt nozzle tip length and atomization gas pressure. As such, the melt nozzle design is a key factor in decreasing the gas flow separation. Parameters such as atomization gas pressure and external design of the melt delivery nozzle can influence the gas separation problem [10] and as a result of this it is important to determine the optimum design for the external melt delivery nozzle geometry.

Mathematical simulation and particularly the use of Computational Fluid Dynamics (CFD) has become a fundamental tool in this analysis and is one of the most practical methods for optimizing the design of close coupled gas atomizers; in particular the design of the melt delivery nozzle geometry and gas die [8,11,12,13]. This approach is now widely used by researchers and commercial atomizer developers to gain an understanding of the gas flow behaviour. Due to the complexity of a two phase simulation of molten metal and gas flow in the vicinity of the melt delivery nozzle most of the numerical modelling is limited to single phase, gas only flow simulation [8,11,12,13], particularly focusing on the design of the gas die. One of the numerical investigations on a discrete gas jet die was a two-dimensional investigation of a single phase compressible gas only flow by Tong et al. [8]. They simulated

two commercial discrete jets and annular slit gas dies on a 2D plane to show the effects on gas flow behaviour around the melt delivery nozzle for the two different gas die systems. Use of CFD approaches, especially single-phase gas only flow modelling, has been shown to provide reliable predictions of the gas flow around the melt delivery nozzle and is a useful tool for helping to solve key gas atomization problems.

A previous numerical study by Aydin et al. [10], for single phase compressible gas flow, investigated gas flow separation with an annular slit C-D gas die and demonstrated that the flow separation alongside a fixed melt nozzle length is strongly influenced by a high atomization gas pressure, with greater boundary layer separation occurring at higher gas pressures. Motaman et al. [14] performed numerical investigations of single phase flow on an annular slit gas jet with four different melt nozzle tip lengths, each with the same external profile. They found that the flow separation for these particular melt delivery nozzles is a function of melt delivery nozzle tip length and atomization gas pressure, with short nozzle lengths and high atomization pressures tending to inhibit flow separation. However, there has been little investigation reported on the discrete jet pressure inversion phenomenon. In this paper we have used both experimental Pulse Laser Imaging technique (PLI) and CFD modelling to investigate the factors that affect, and the mechanisms behind, the discrete jet pressure inversion effect.

2. Experimental procedure

Fig.3 shows a schematic design of the melt delivery nozzle considered in this study. Four different melt delivery nozzles were used in this test with different gas jet mis-match angles (relative to melt delivery external wall). The mis-match angle of (α) is the measured angle between melt nozzle external wall and the gas jet direction. The details of the mis-match angle and the melt tip diameter for the series of investigated melt nozzles are given in Table 1. A series of experimental tests were carried out with an analogue water atomizer with each of the four different melt delivery nozzle types using an 18 holes discrete gas jet die configuration with C-D gas chamber profile [5]. The gas die was designed (based on isentropic flow) to operate at a pressure of 2.7 MPa and an exit velocity of Mach 2.6. The details of the C-D gas jet profile are given in Fig. 4.

Four different melt delivery nozzles were made from brass with dimensions as given in Table 1. The analogue atomizer used water from a header tank via a regular heating pump at a constant pressure of around 4 MPa. Air was used as the atomizing gas which was supplied from 4 standard compressed air bottles. A Pulse Laser Imaging (PLI) technique was employed for filming the back-stream flow phenomenon during the water atomization. PLI is an imaging technique which operates by producing a double pulse laser beam which can be used to create two consecutive images split by a very short time delay. Due to a short exposure time of around 15 μs between each laser pulse, and the use of a high resolution imaging technique, the back-stream flow of water moving into the negative pressure zone at the outer surface of the melt delivery nozzle can be visualized during the atomization of the water using the different nozzles. A schematic view of the analogue water atomizer and the PLI system setup is shown in Fig. 5a: (1) is the laser beam source, (2) the telescopic optical arm which guides the laser beam to the test area, (3) the analogue atomizer box. This box is made from anodised aluminium to prevent the laser beam exiting the testing area. The laser is an Nd: YAG type with energy of 90mj/pulse, wave length of 532 nm and pulse duration of 6ns. The PLI images were captured for analysis using a two megapixel camera that is specially designed for this system [5].

3. Numerical model procedure

In this research a detailed Computational Fluid Dynamic (CFD) study has been conducted of the high-speed gas flow around each of the four nozzle designs. As the flow is supersonic the gas is required to be modelled as a compressible fluid and as such conservation equations for continuity, momentum and energy are all solved. For each study, a single phase steady-state flow field is simulated based on solving the Reynolds Averaged Navier Stokes (RANS) equations. Since the flow is in the turbulent regime, the k-ω model has been applied to close the Reynolds stress terms in the (RANS) equations [6]. The k-ω model has been validated for high speed internal flows and has been shown to give good predictions for the associated shocks [14]. Furthermore, both k-ε and *k*-ω turbulence models were applied during the investigation and the results were shown to be relatively insensitive to this change. This provided further confidence in the use of the k-ω model. The result of using these two turbulence models (for nozzle type 1 at a gas pressure of 1MPa) is presented in section 4 and Fig 10. The (RANS) equations are solved numerical using the finite volume solver ANSYS Fluent 13. The mathematical domain is such that gas exiting the chamber is travelling in the x direction. The SIMPLE algorithm with an implicit 2^{nd} order upwind scheme is used to solve the RANS equations in the computational domain shown in Fig. 5b (for a single phase compressible gas, air).

It should be noted the mathematical model omits the molten metal as the aim of this study is to understand the simplified situation of the high-velocity gas flow behaviour exiting the different nozzle designs**.** Furthermore, the model represents a discrete jet C-D gas die**.** The model domain was solved in the r-z components of a cylindrical system which is independent of φ (i.e. a 2D axis-symmetric domain is considered which approximates the 3D flow). This is considered valid because when observing the Schlieren images of the gas flow from the gas

only phase of atomiser it is apparent, that although using 18 discrete jets, the resultant combination of jets form an approximately uniform radial profile [8]. As such, for the CFD model the assumption that the flow can be approximated by a radially axisymmetric flow is taken. The assumption that gravity can be neglected is also made. This is supported through experiments where the orientation of the atomizer is typically not considered to have a noticeable impact on the atomisation results. To further confirm this, a test case including gravity (acting perpendicular to the jet direction) was run with the same numerical domain and at a gas pressure of 1 MPa. No significant difference was observed between the predicted results and the result from the model without gravity. In order to establish the numerical simulation of the gas flow and to simplify the numerical calculations, the following further assumptions also have been made:

1- Flow is considered to be steady-state.

2- Flow is considered 2D axis-symmetric.

3-The fluid is considered as air and modelled as a compressible ideal gas.

4-The impact of the molten metal is not considered.

3.1. Boundary conditions

Different atomization gas pressures at the entrance of the C-D gas die inlet chamber were investigated ranging from those expected to produce over-expanded flow (1, 2 MPa), ideal flow (3 MPa) and under-expanded flow (4 and 5 MPa). The outlet of the domain (downstream of the nozzle) was taken as a pressure condition at atmospheric pressure. Also for the inlet to the nozzle chamber, the inlet boundary condition was modelled as a pressure inlet with the pressure determined based on experimental data. The outer boundary of the chamber, melt nozzle and gas die wall were taken as walls with a no-slip velocity condition. Moreover, the boundary labelled ‘upper domain boundary’ in Fig. 5b was also modelled as a wall with a no-slip condition. It is noted that in preliminary modelling domain sensitivity studies two different boundary conditions (atmospheric pressure and slip-wall conditions) were applied (separately) to the upper domain boundary condition to investigate the sensitivity of each boundary condition on flow predictions. When considering the boundary as a zero pressure condition it was found there was minimal flow across this boundary. Furthermore, when solving with the slip-wall condition implemented, it was shown that the flow field was the same as with the pressure condition applied. As such, for convenience the slip-wall condition was implemented for all later studies as it provided improved convergence and stability. Furthermore, for the energy boundary conditions, the gas temperature for the upper boundary flow inlet and exit were set at a constant temperature of 300 K. Table 2 shows an overview of the boundary conditions.

3.2. Domain and mesh independence study

The final geometry that was constructed and implemented was demonstrated to be domain independent. Furthermore, to ensure the results were independent of both the domain size and boundary locations a detailed study was undertaken to identify the impact of moving the inlet/outlet boundaries and size of the computational domain. A series of high-quality mesh were developed of increasing fineness to evaluate the impact on the results (Fig. 6). Three meshes of increasing fineness were used in the work (mesh 1, 9000 elements, mesh 2, 11000 elements and mesh 3, 18000 elements). To determine the influence of mesh refinement on the CFD solution and to ensure mesh independence, before proceeding to the numerical simulations, the velocity and pressure were monitored along the vertical lines AB and CD (Fig. 5b) which are at locations 0.4 mm before the front of the melt nozzle tip and 3 mm following the melt nozzle tip, respectively. The velocity variations along these two lines for each of the different mesh are shown in Fig. 7 and 8. The velocity field for mesh 2 and 3 were judged to be mesh independent and as such it was appropriate to use mesh 2 for the numerical experiments.

4. Results and discussion

Fig. 9 shows a close-up PLI image of the four different melt delivery nozzles during the atomization of water with analogue atomizer at an atomization gas pressure of 1 MPa and a distance between the discrete C-D gas exit jets and the outer wall of the melt nozzle of 1.65 mm [5]. In these images the atomized fluid appear bright due to the reflected laser light as, due to the illumination angle, does the right hand side of the melt nozzle. The whole of the base of the nozzle is wet with the second fluid (pre-filming) as can clearly be seen in the images. For nozzle type 1, with lowest melt nozzle wall inclination, corresponding to no angular mis-match between the gas jets and the melt nozzle, significant back-streaming of the atomized fluid is apparent. The amount of back-stream flow decreases with an increase in the angular mis-match of the melt nozzle (increasing the mis-match between the gas jets and the nozzle so the gas flow is inclined in towards the nozzle). For nozzle types 3 and 4 no back-stream flow was observed. In an attempt to explain this phenomenon observed in the discrete jet gas set up, CFD modelling has been undertaken to provide further understanding of the gas boundary layer behaviour around the melt delivery external wall.

Fig. 10 illustrates the numerical result for the total pressure contour for melt nozzle type 1 with a 1.65 mm C-D gas die exit distance from melt nozzle wall at the gas pressure of 1 MPa. The results are shown for two different turbulence models, k-ε and k-ω as outlined in section 3. The results when using these two models are very close for this flow (they are judged to be identical from the point of view of the flow behaviour and the length of negative pressure zone). The velocity predictions when using the k-ω turbulence model for the full modelling domain (for the same nozzle and inlet pressure) are shown in Fig. 11.

The total pressure contour for the four melt nozzles at the same gas pressure is given in Fig. 12. As a consequence of the flow being overexpanded when it leaves the gas jet we observed the flow expanding as the gas leaves the C-D nozzle area. The negative pressure zone is a dark blue zone at this image. The region of sub-ambient pressure causes the liquid metal to be drawn from the tip of the melt nozzle up its outer surface. The molten metal is then exposed to a very cold gas jet from the gas die and solidifies rapidly and accumulates around the outer surface of the melt delivery nozzle. This will alter the shape of the melt delivery nozzle and clog the gas jets on the die, halting the atomization process. For better observation of back-stream flow phenomenon at the negative pressure zone, Fig. 13 shows a close up of the velocity field around the external wall of the different melt nozzles. The colour of the vectors indicates the velocity magnitude and the end of the gas recirculation region for each nozzle is shown in this figure with an arrow. For nozzle type 1, the end of the recirculation region (closest to the tip edge) reaches to a point around 0.1 mm from the tip edge of the melt delivery nozzle. The arrow in the Fig. 13 indicates the point at which there is a change in direction of the recirculating flow close to the external wall of melt delivery nozzle in the negative pressure zone. This situation arises due to the negative pressure zone. For nozzle type 2, the equivalent recirculation zone ends at a distance 0.7 mm from the melt nozzle tip edge. This point for nozzle types 3 and 4 occurs at a distance 0.93 and 1.2 mm from melt nozzle tip edge, respectively. By comparison with the PLI images shown in Fig. 9 it is anticipated that for nozzle type 2 the recirculation region that ends 0.7 mm from the melt nozzle tip would give rise to marginal back streaming behaviour as the recirculating flow in this case would be just isolated from the atomisation region. It can be observed that with moving from melt nozzle type 1 to type 4 at the atomization gas pressure of 1 MPa, the position of the end of the recirculation region moves further away from the nozzle tip. This indicates that the suction, which results in back-streaming of the melt, appears to reduce as the angular mis-match between the gas jets and the melt nozzle external wall increases.

Fig. 14 illustrates the velocity field for all four melt nozzles at an atomization gas pressure of 2 MPa. For nozzle type 1, except for a small recirculation zone that occurs at the corner of melt delivery nozzle wall, all of the velocity vectors in the boundary region are parallel to the melt nozzle wall. The same situation was also seen for the other nozzles at 2 MPa and for all the nozzles at higher gas pressures. However, in the analogue atomizer, back-streaming was still seen, albeit at a reduced rate, at 2 MPa. We speculate that this is because a layer of stationary gas adhering to the inner walls of the jet reduces the bore of the jet, effectively increasing the ratio of outlet area to throat area and hence shifting the ideal operating pressure for the die to higher pressures.

In increasing the atomization gas pressure to 3 MPa, slightly above the design criterion for the C-D gas die, the gas showed under-expanded behaviour and a velocity of Mach 2.6. No sign of back-stream flow was observed near the melt tip for any of the melt nozzles at the higher gas atomization pressures of 3, 4 and 5 MPa due to under-expanded gas jet flow where the gas flow expansion is behaving more like a choked jet. Under the conditions considered here we therefore conclude that increasing the gas pressure beyond 1 MPa, the chance of back-stream flow for these four different melt delivery nozzles is significantly reduced. This

situation occurs due to the gas being under-expanded when exiting the C-D jet, wherein further expansion will occur beyond the exit such that no negative pressure region occurs near the external wall of the melt delivery nozzle. In accordance with the above mentioned results, the CFD results and commonly observed experience, back-stream flow is unlikely to occur for a closed coupled gas atomizer with cylindrical gas jets. This is due to the choked nozzle which causes there to be under-expanded flow at the nozzle exit which in turn gives rise to rapid expansion of the gas upon exiting the die.

We hypothesis that for nozzle types 1 and 2 at an atomization gas pressure of 1 MPa the back-stream flow is happen due to the physical distance between the position of exit jet of C-D gas die and external wall of melt delivery nozzle. This phenomenon was not observed in the case of flow separation phenomenon in which the gas boundary layer separation is highly related to the gas travel distance or melt delivery tip length where the greater given distance to the boundary layer flow distance, the greater flow separation that occurs [15].

So decreasing the distance between the exit of the gas jet and the external wall of the melt delivery nozzle has been proposed by authors as a means of mitigating the back-streaming phenomenon. In order to investigate the effect of this separation on the back-flow and determining the maximum distance at which no back-stream flow will occur, the position of C-D gas exit jet has been changed to 1.6, 1.55, 1.5, 1.45 and 1.40 mm from external wall of melt nozzle in turn, for all four nozzles at an atomization gas pressure of 1MPa.

As described above, by comparison of the PLI images and the CFD results we have taken the criterion for identifying back-stream flow in the CFD simulations as the sub-ambient pressure zone approaching within 0.7 mm of the melt nozzle tip. According to this criterion, at gas exit jet distances of 1.6 mm, strong back-stream flow occurred for nozzle type 1 at an atomization gas pressure of 1 MPa due to the negative pressure zone adjacent to the outer wall of the melt delivery nozzle. The distance to this negative pressure region was measured at around 0.1 mm from the tip of the melt delivery nozzle. The negative pressure zone at C-D gas exit jet distance of 1.6 mm for nozzle types 2, 3 and 4 was observed at 0.8, 1 and 1.2 mm, respectively, from melt delivery nozzle tip, wherein we conclude that back-stream flow was unlikely to occur for any of these melt nozzles.

For nozzle types 2, 3 and 4 with gas exit jet distance of 1.55 mm and at gas atomization pressure of 1 MPa, the chance of back-stream flow was also thought to be unlikely due to position of gas jet exit distance from melt delivery tip, but for nozzle type 1 the negative pressure zone was took place about 0.28 mm from melt nozzle tip and it is therefore likely that this will still causes a strong back-stream flow.

Fig.15 shows the total pressure contour of four melt nozzles at atomization gas pressure of 1 MPa with C-D gas jet exit distance of 1.5 mm. For nozzle types 1 and 2, the negative pressure zone occurs at 0.57 and 1.31 mm from melt delivery tip respectively, while for nozzle types 3 and 4 the corresponding values were 1.63 mm and 1.65 mm from melt nozzle tip. The chance of back-stream flow still exists for nozzle type 1 due to the negative pressure zone being within 0.57 mm of melt nozzle tip. With decreasing the gas jet exit distance from

1.65 mm to 1.5 mm for nozzle types 2, 3 and 4 the negative pressure zone was measured at a more distance from melt delivery tip and with increasing the gas jet mis-match angle, this negative pressure zone is become smaller and the effect of back-stream flow is significantly decreased.

For a distance between the C-D jet and the external melt nozzle wall of 1.45 mm the adverse pressure zone was measured to begin around 0.7 mm from melt nozzle tip edge of a type 1 nozzle at atomization gas pressure of 1 MPa. This is equal to the limit of a weak stream flow occurrence. No back stream-flow is expected for the rest of melt nozzles. In addition, when decreasing the gas jet exit distance to 1.4 mm, back-stream flow is not expected to be a problem with any melt nozzle type. It was therefore decided to measure the maximum limitation in which this phenomenon can occur between the condition of weak to no back-stream flow, particularly for nozzle types 1 and 2. Consequently, the gas jet exit distance of 1.64 mm and 1.44 mm from external melt delivery nozzle was numerically tested to identify this limitation.

At gas jet exit distance of 1.44 mm, the adverse pressure zone was moved to 0.91 mm from melt nozzle tip edge for nozzle type 1 and for gas exit distance of 1.64 mm this region was placed at 0.73 mm for nozzle type 2. So the maximum gas jet exit distance limitation in which no back-stream flow was predicted for nozzle type 1 and type 2 was obtained at 1.44 mm and 1.64 mm, respectively from melt nozzle external wall. At higher atomization gas pressure of 1 MPa like previous condition, no back-stream flow was expected for these two nozzles. For the rest of three melt nozzle types, the negative pressure zone was placed at a distance more than 0.7 mm from melt tip and no back-stream flow is unlikely. The relation between different melt delivery nozzle type and C-D gas jet exit distance from external wall of the melt nozzle on back-stream flow phenomenon is given on table 3.

5. Conclusions

In this paper the effect of changing the angular mis-match between the external wall of melt delivery nozzle and the line of the gas jets on back-stream flow phenomenon with a C-D discrete gas die was numerically investigated. The results were compared with experimental PLI images obtained with an analogue water atomizer. The results of numerical results of single phase gas only flow predicted that for discrete C-D gas die with exit distance of 1.65 mm, the nozzle type 1 with lowest mis-match angle can cause the highest back-stream flow around external melt delivery nozzle at atomization gas pressure of 1 MPa. The back-stream flow for nozzle type 1 was measured at 0.1 mm from the tip of melt delivery nozzle and for nozzle types 2, 3 and 4 this distance was observed at 0.7, 0.93 and 1.2 mm from melt nozzle tip edge, respectively. This situation was also approved by PLI images technique that obtained with the same melt nozzle geometry and C-D gas die set up with an analogue atomizer with two phase fluid. With increasing the mis-match angle this effect decreased and no back-stream flow was observed for nozzle type 3 and 4. In addition, the effect was totally suppressed at gas pressures above 1 MPa for these particular melt nozzle designs.

For a C-D discrete gas die design, operating in the under-expanded gas flow condition no negative pressure was seen close to the external wall of the melt nozzle. It was confirmed that at atomization gas pressures above of 1 MPa, the high velocity gas boundary layers are almost parallel to the external wall for all four melt nozzles. Moreover, decreasing the distance between the gas jets and the wall of melt delivery nozzle could sharply reduce the back-stream (DJPI) effect for nozzle types 1 and 2. The maximum gas jet exit distance in which no back-stream flow was predicted for nozzle type 1 was 1.45 mm and this number for nozzle type 2, was 1.64 mm. No back-stream flow was observed for nozzle types 3 and 4 at any atomization gas pressure with different C-D gas exit jet distance from melt nozzle external wall.

References

[1] Ting. J, Anderson. I. E, Terpstra. V. R and Mi. J, Design and testing of an improved convergent–divergent discrete-jet high pressure gas atomization nozzle. Advances in powder metallurgy and particulate materials in: J.J. Oakes, J.H. Reinshagen (Eds.) 1998; APMI-MPIF; vol. 3; Part 10; Princeton; NJ; 1998; 29–39.

[2] Grant. P. S, Solidification in spray forming. Metallurgical and Materials Transactions A; 2005; vol. 38; 1520-1529.

[3] Mullis. A. M, Adkins. N. E, Aslam. Z, McCarthy I. N. and Cochrane. R.F, High frame rate analysis of the spray cone geometry during close-coupled gas atomization. International Journal of Powder Metallurgy; 2008; 44; 55-64.

[4] Mullis. A. M, McCarthy I. N and Cochrane R. F, High speed imaging of the flow during close-coupled gas atomisation: Effect of melt delivery nozzle geometry. Journal of Materials Processing Technology; 2011; 211; 1471-1477.

[5] McCarthy. Ian. N, Optical investigation into close-coupled gas atomization. PhD thises,Institute for materials research;University of Leeds;September 2010.

[6] F. Menter. Two-equation eddy-viscosity turbulence models for engineering applications. Author: Menter, F. R. Published in; AIAA Journal; 1994; vol. 32; No. 8; 1598.

[7] Otaigbe. J, and Mcavoy. J, Gas atomization of polymers. Advances in polymer Technology; 1998; No. 20; 145-160.

[8] Mingming Tong, David J. Browne, Modelling compressible gas flow near the nozzle of a gas atomiser using a new unified model. Computers and fluids; Vol. 38; Issue 6; June 2009; 1183–1190.

[9] Unal. R, Investigation of the metal powder production efficiency of a new convergent-divergent nozzle in close-coupled gas atomization. Powder Metal; 2007; 302-306.

[10] Ozer Aydin, Rahmi Unal. Experimental and numerical modelling of the gas atomization nozzle for gas flow behaviour; Computers and Fluids; 2011; No. 42; 37–43.

[11] Mi. J, Figliola. R. S and Anderson. I. E, A numerical investigation of gas flow effects on high pressure gas atomization due to melt tip geometry variation. Metallurgical and Materials Transactions B; vol. 28B; 1997; 935-941.

[12] Zeoli. N, Gu. S, Computational validation of an isentropic plug nozzle design for gas atomization. Computational Materials Science; 2008; No 42; 245–258.

[13] Zeoli. N, Gu. S, Numerical modelling of droplet break-up for gas atomisation. Computational Materials Science; 2006; No 38; 282–292.

[14] Motaman. S, Mullis. A. M, Cochrane. R and Borman. D, The effect of melt nozzle geometry on close –coupled gas atomization. International Conference on Powder Metallurgy & Particulate Materials 2012; 10-13 June 2012, Nashville, TN, CD proceedings ISBN: 978-9853397-2-2; MPIF 2012; 02/01-02/12.

[15] Motaman. S, Mullis. A. M, Cochrane. R and Borman. D, Use of computational modelling for investigation the Effect of melt delivery nozzle tip length on gas flow separation in supersonic gas atomization. ICLASS; 12th Triennial International Conference on Liquid Atomization and Spray Systems; Heidelberg; Germany; September 2012.

Fig. 1. A ceramic melt delivery nozzle failed due to back-streaming phenomena during gas atomization of Ni-Al [5].

Fig. 2. Schematic view of A: Discrete Jet Pressure Inversion (DJPI) and B: gas flow separation mechanism.

Fig. 3. Melt delivery nozzle design and dimensions (mm).

Fig. 4. Schematic view of C-D gas jet chamber design.

Fig. 5. a: Schematic setup of analogue water atomizer and PLI system, b: Computational domain and boundary conditions.

Fig. 6. An example of the computational mesh in the vicinity of the melt nozzle tip and C-D gas die.

Fig. 7. The influence of mesh size on the predicted velocity magnitude along line AB.

Fig. 8. The influence of mesh size on the predicted velocity magnitude along line CD.

Fig. 9. PLI image of back-stream flow at gas pressure of 1 MPa with analogue atomizer for different melt delivery nozzle incline wall angle (arrows indicate the back-stream flow around melt tip external wall) [5].

Fig. 10. Total presure countour (Pa) for nozzle type 1 at atomization gas pressure of 1MPa with a: k-ε turbulence model, b: k-ω turbulence model.

Fig. 11. Velocity countour (m s^{-1}) for nozzle type 1 at gas pressure of 1 MPa with k-ω turbulence model.

Fig. 12. Total pressure contour (Pa) and negative pressure zone of different melt nozzles at atomization gas pressure of 1 MPa and 1.65 mm gas jet distance from melt delivery external wall.

Fig. 13. Velocity vector field (m s^{-1}) around melt nozzle external wall for different melt nozzles at atomization gas pressure of 1MPa and gas exit jet distance of 1.65 mm.

Fig. 14. Velocity vector field (m s^{-1}) for different melt nozzle types at atomization gas pressure of 2 MPa and gas exit jet distance of 1.65 mm.

Fig. 15. Total pressure contour (Pa) and negative pressure zone of different melt nozzles at atomization gas pressure of 1MPa and 1.5 mm gas jet distance from melt delivery external wall.

Table 1. Melt delivery nozzle geometry details.

Table 2. An over view summery of the boundary conditions.

Table 3. Relationship between back-streaming flow and nozzle design parameters.

Table 1

Nozzle type	Type 1	Type 2	Type 3	Type 4
a: Tip length (mm)	6	6	6	6
b : Tip base diameter (mm)	5	5.6	6.1	6.6
α: Mis-match angle (degree)	0	3	5	7

Table 2

Type	Boundary condition (momentum)	Boundary condition (energy)
Inlet nozzle chamber	Pressure inlet (determined from experimental test pressure)	300 k
Downstream outlet	Pressure outlet (atmosphere)	300 k (for backflow)
Chamber, melt nozzle and gas die wall	No-slip wall	Insulating condition
Upper domain boundary	No-slip wall	300 k

Table 3

Nozzle Type / C-D exit distance (mm)	Type 1	Type 2	Type 3	Type 4
1.65	Strong	Weak	None	None
1.64	Strong	None	None	None
1.6	Strong	None	None	None
1.55	Strong	None	None	None
1.5	Strong	None	None	None
1.45	Weak	None	None	None
1.44	None	None	None	None
1.4	None	None	None	None

Figure 1

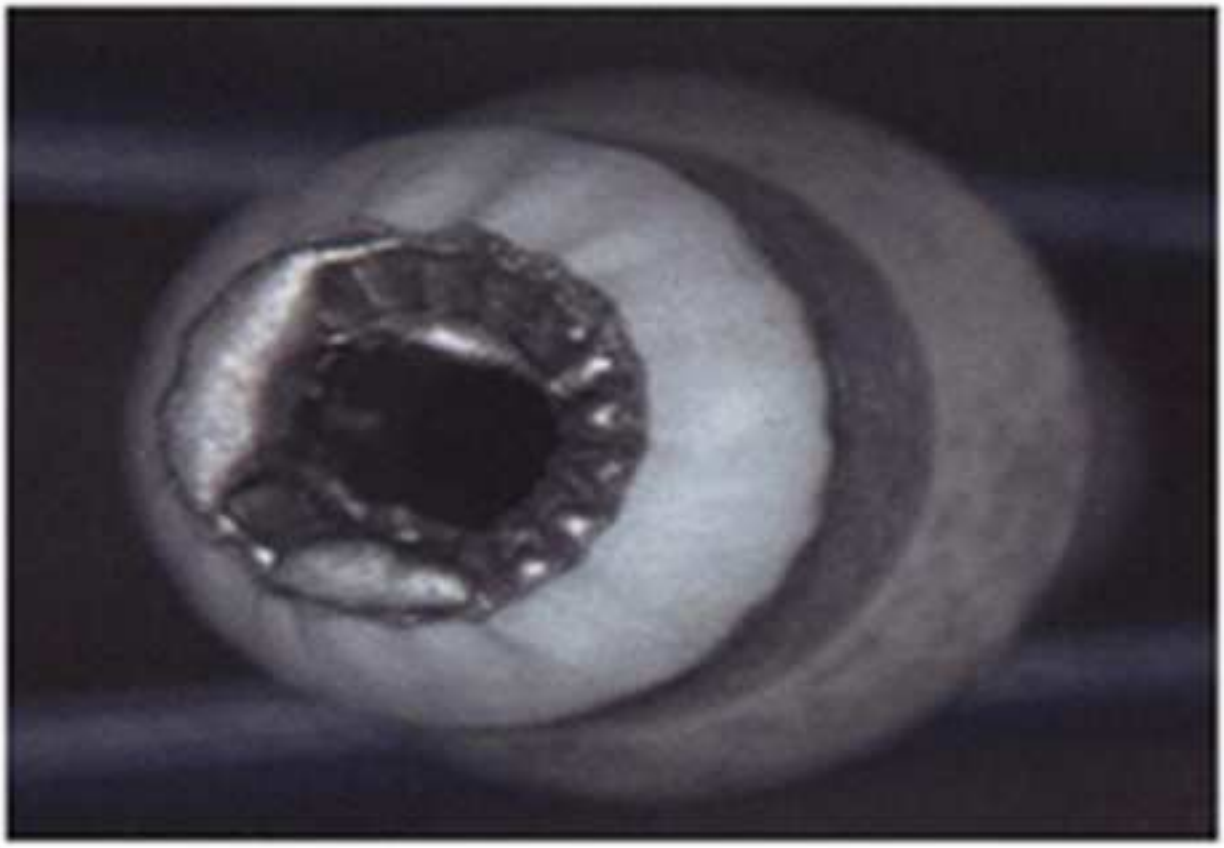

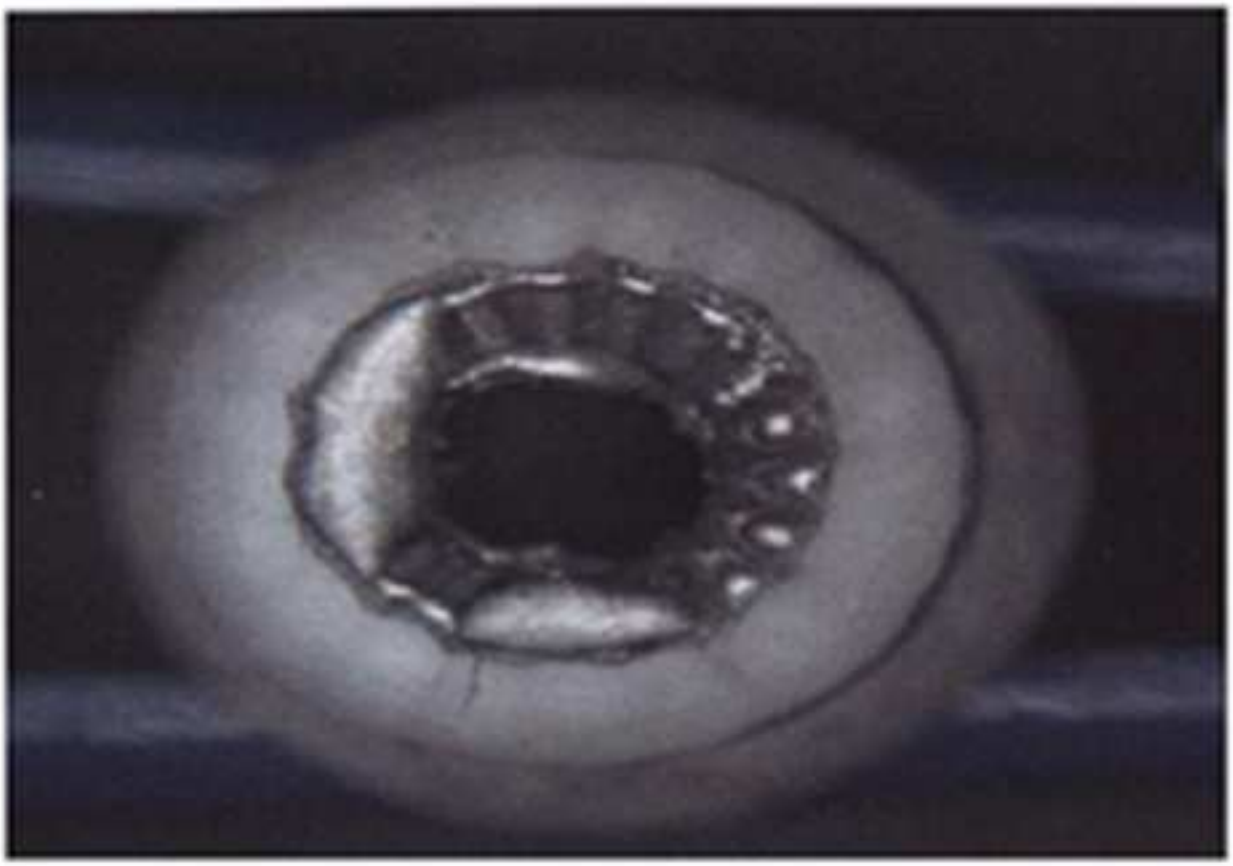

Figure 2

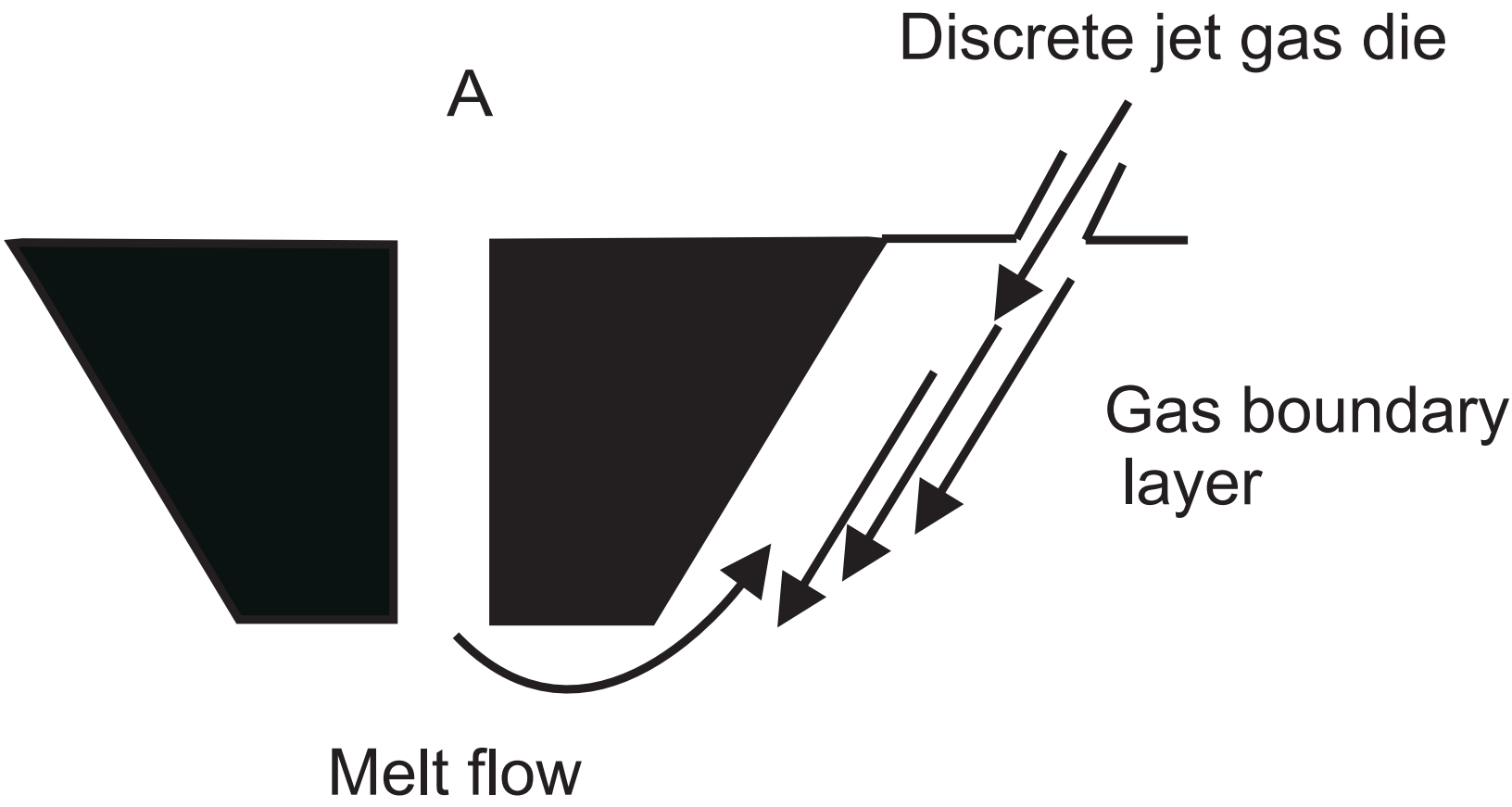
Discrete jet gas die
A
Gas boundary
layer
Melt flow

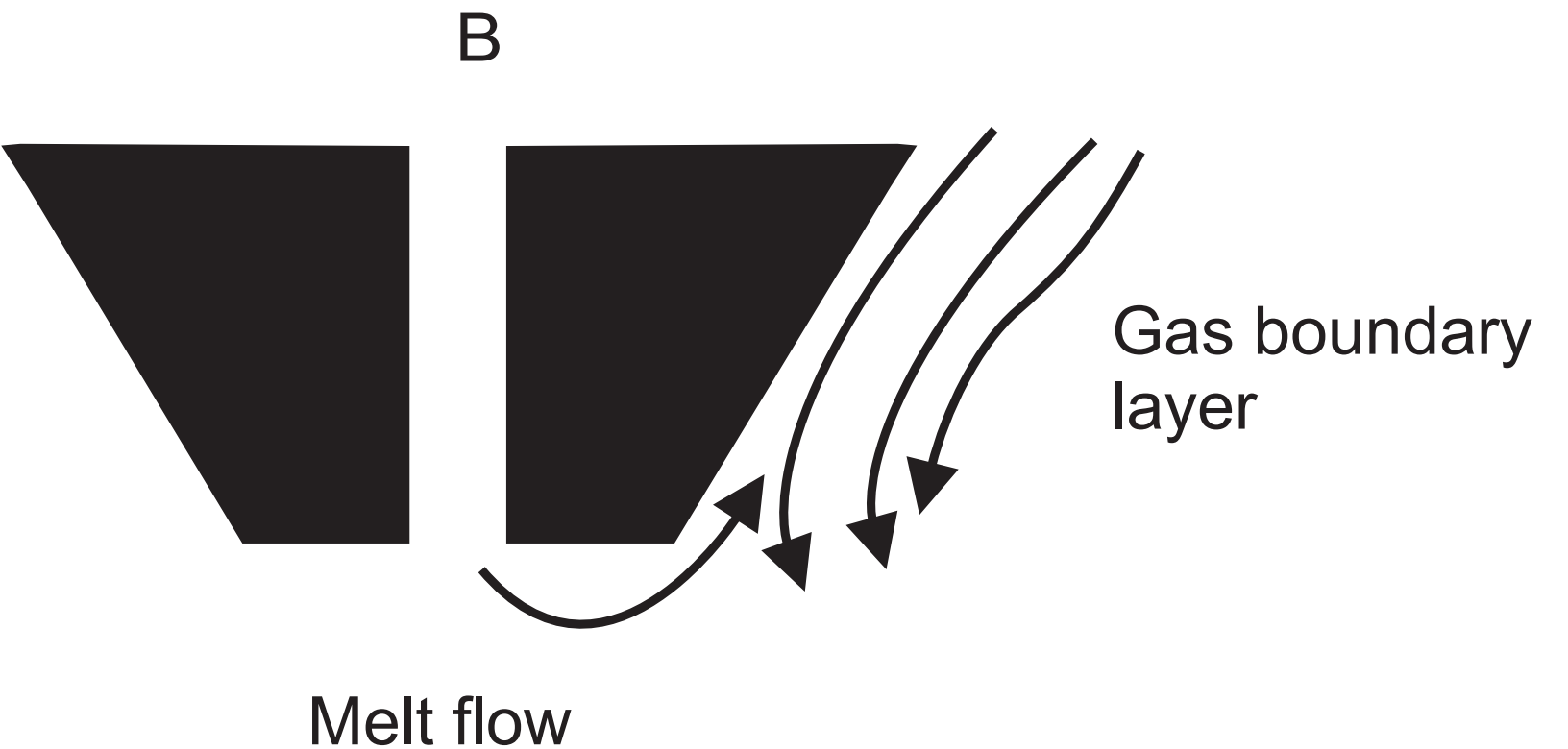
B
Gas boundary
layer
Melt flow

Figure 3

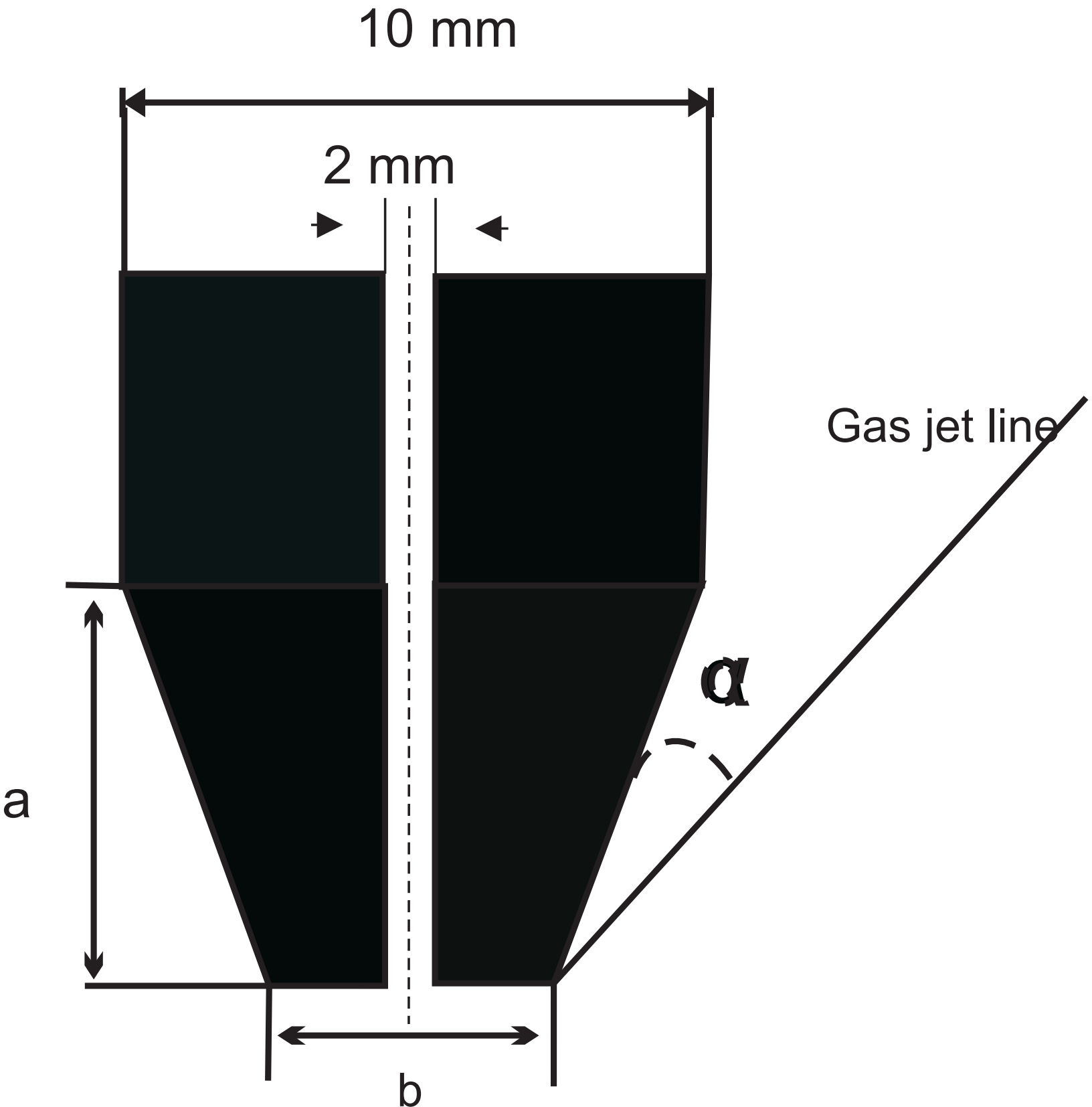

Figure 4

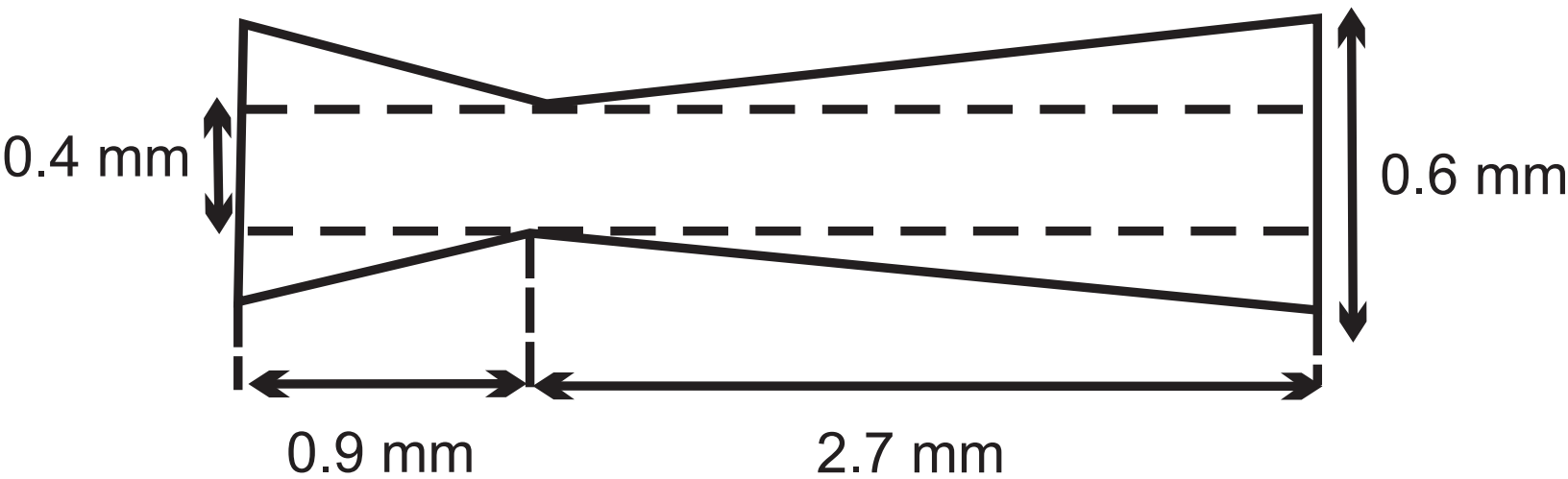

Figure 5

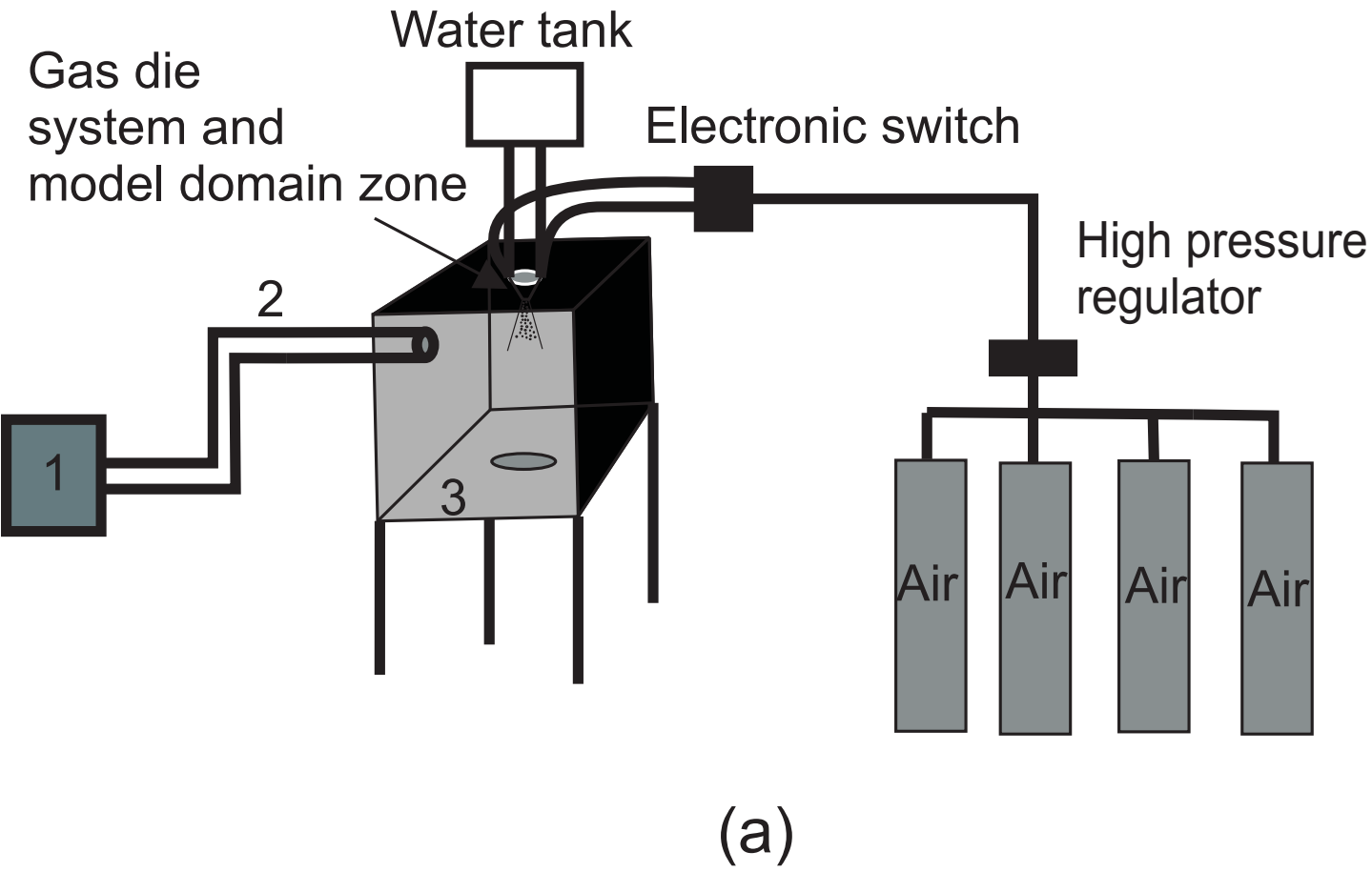
Water tank
Gas die
system and
model domain zone
Electronic switch
High pressure
regulator
2
1
3
Air
Air
Air
Air

(a)

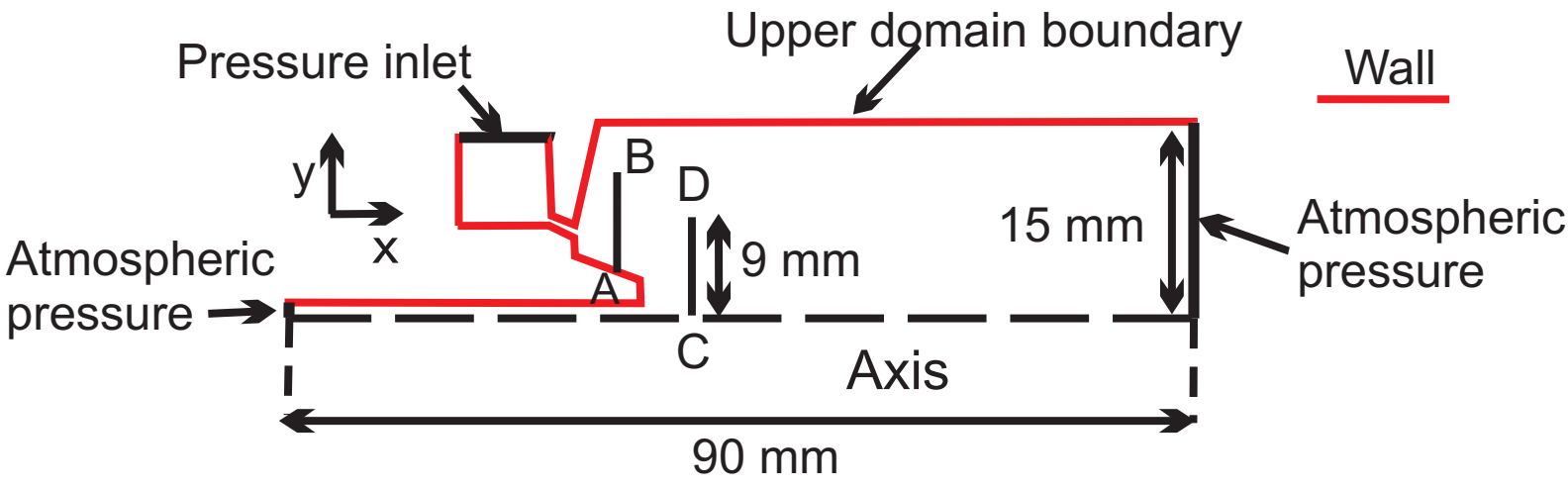
Upper domain boundary
Wall
Pressure inlet
y
x
B
D
A
C
9 mm
15 mm
Atmospheric
pressure
Atmospheric
pressure
Axis
90 mm

(b)

Figure 6

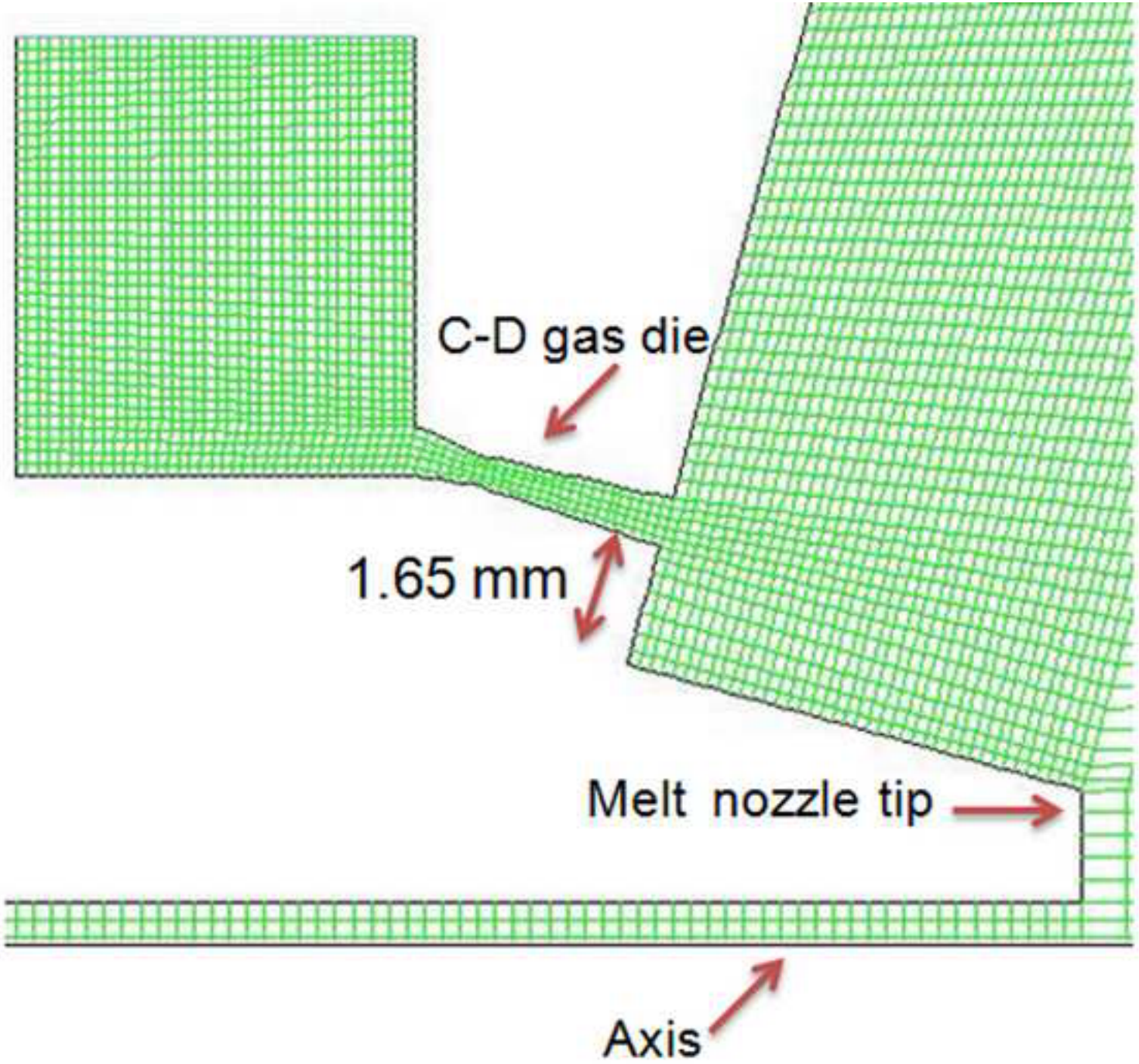

Figure 7

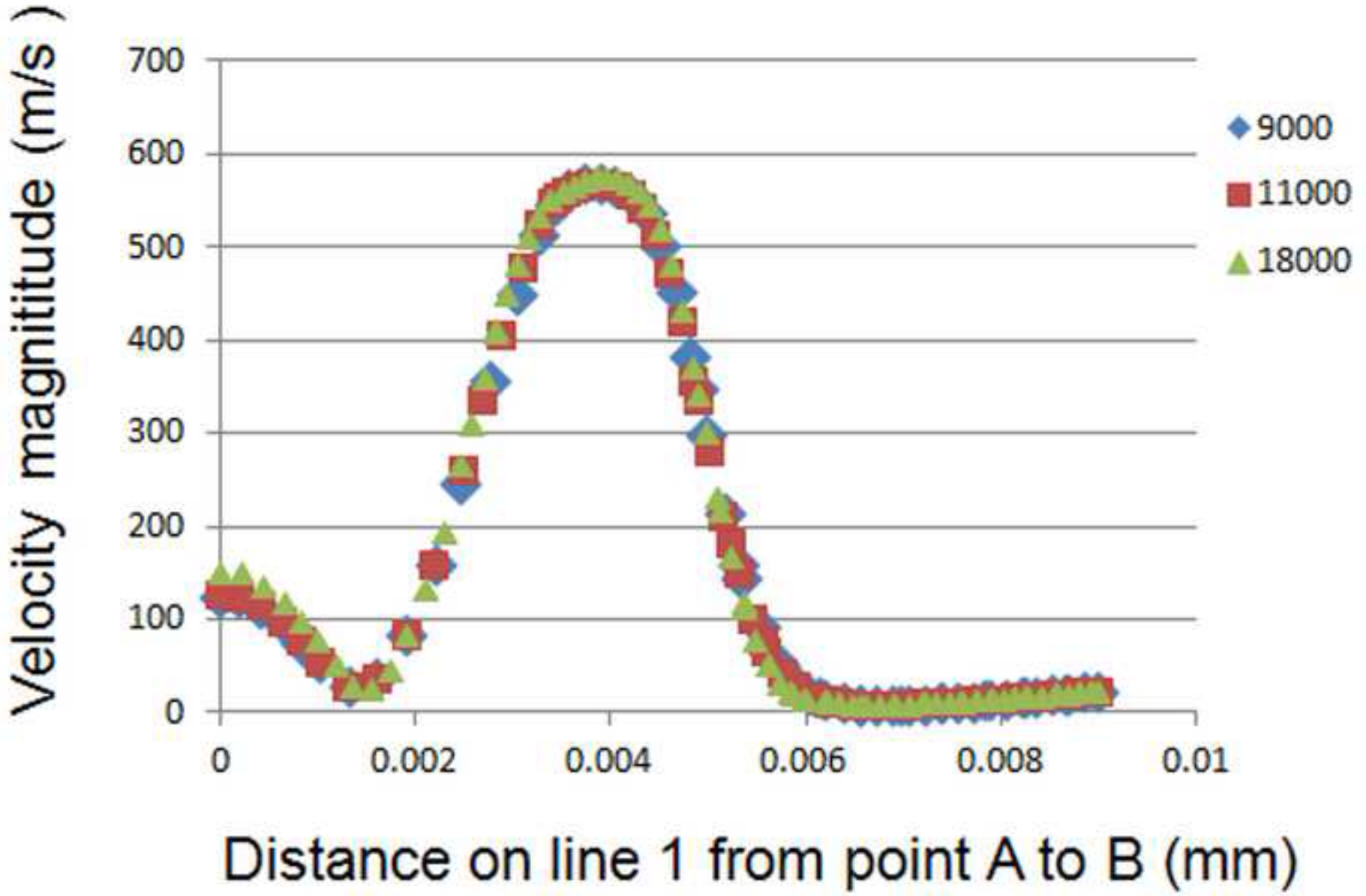
Velocity magnitude (m/s)
700
600
500
400
300
200
100
0
0
0.002
0.004
0.006
0.008
0.01
9000
11000
18000
Distance on line 1 from point A to B (mm)

Figure 8

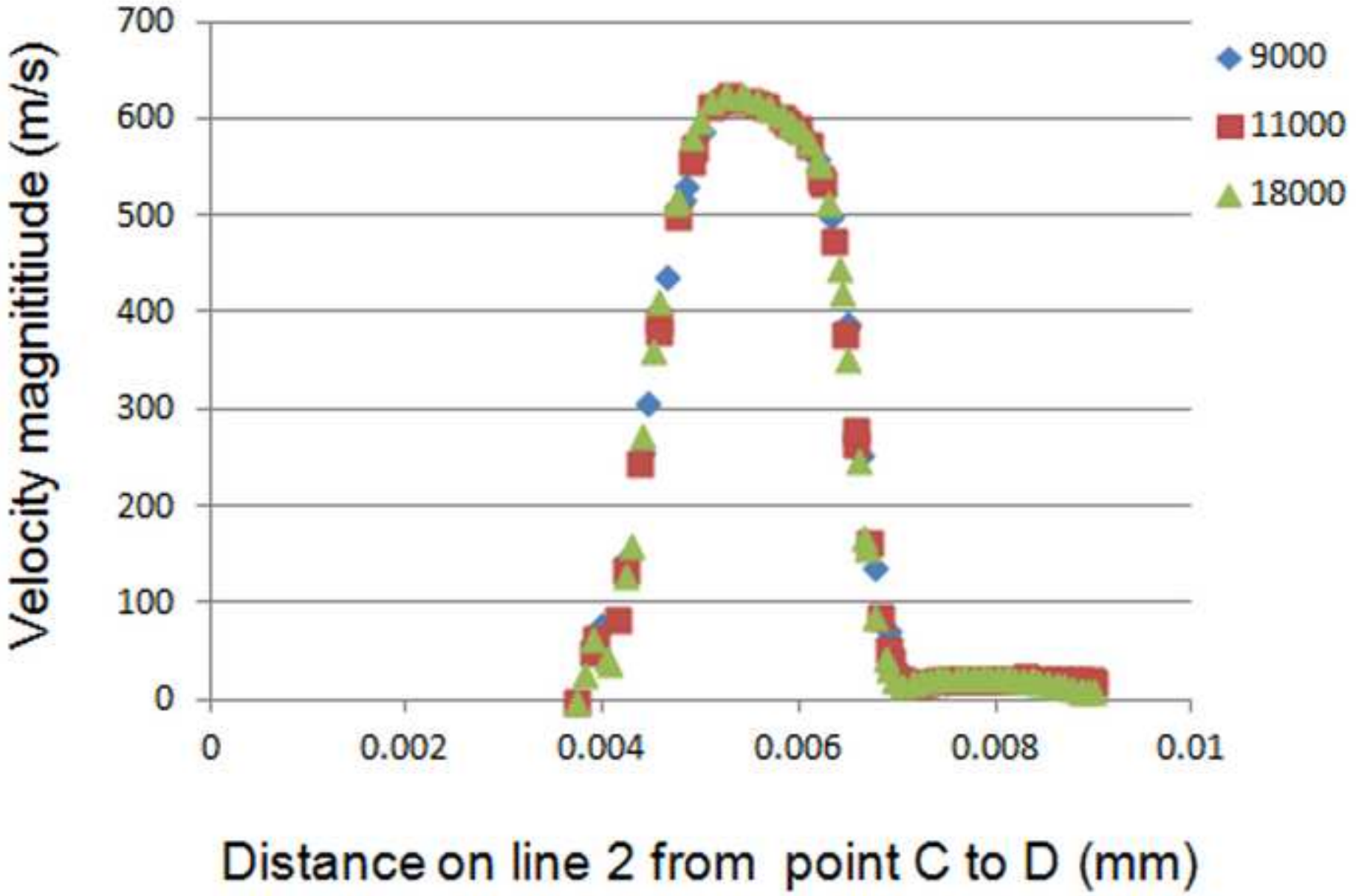
Velocity magnitiude (m/s)
700
600
500
400
300
200
100
0
0
0.002
0.004
0.006
0.008
0.01
9000
11000
18000
Distance on line 2 from point C to D (mm)

Figure 9

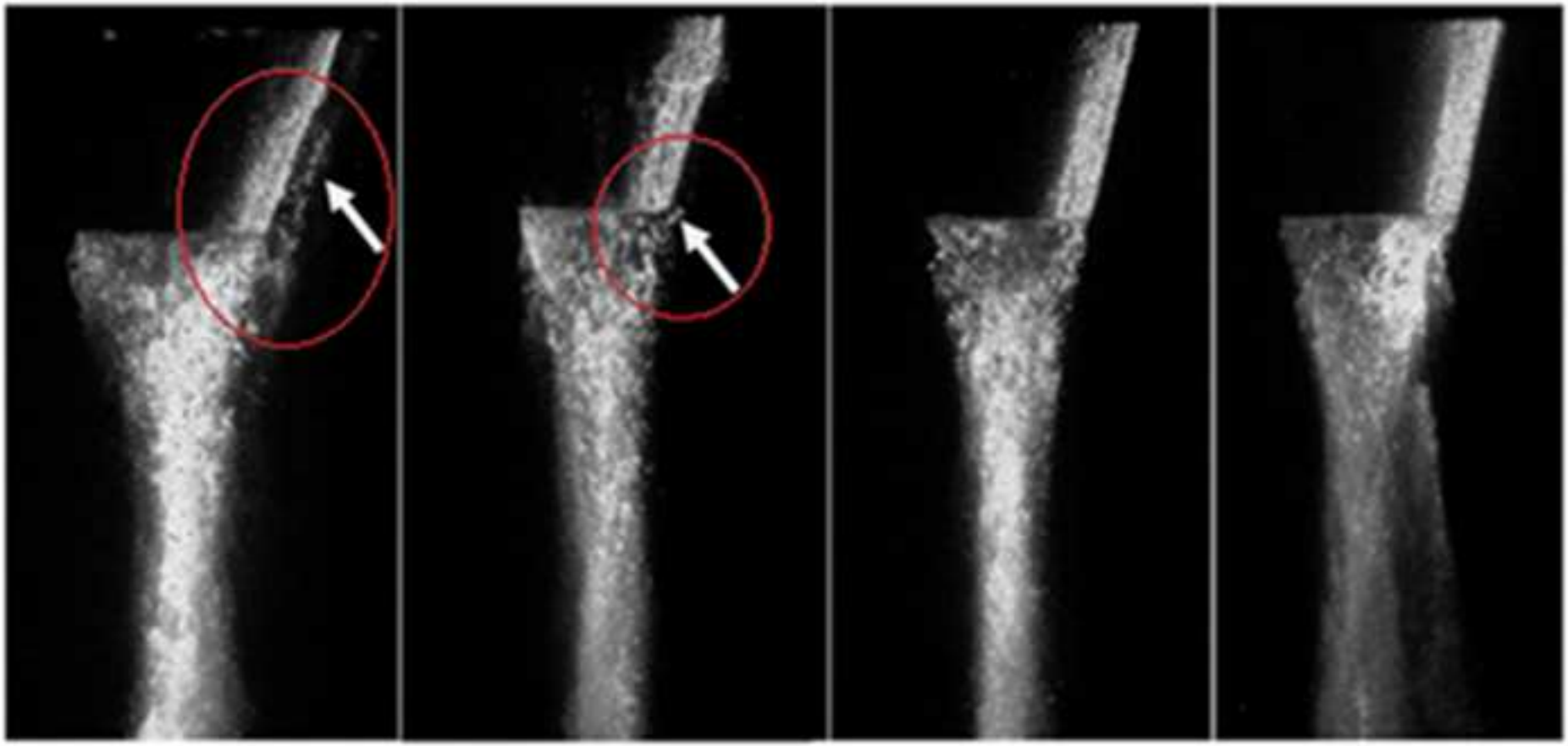

Figure 10

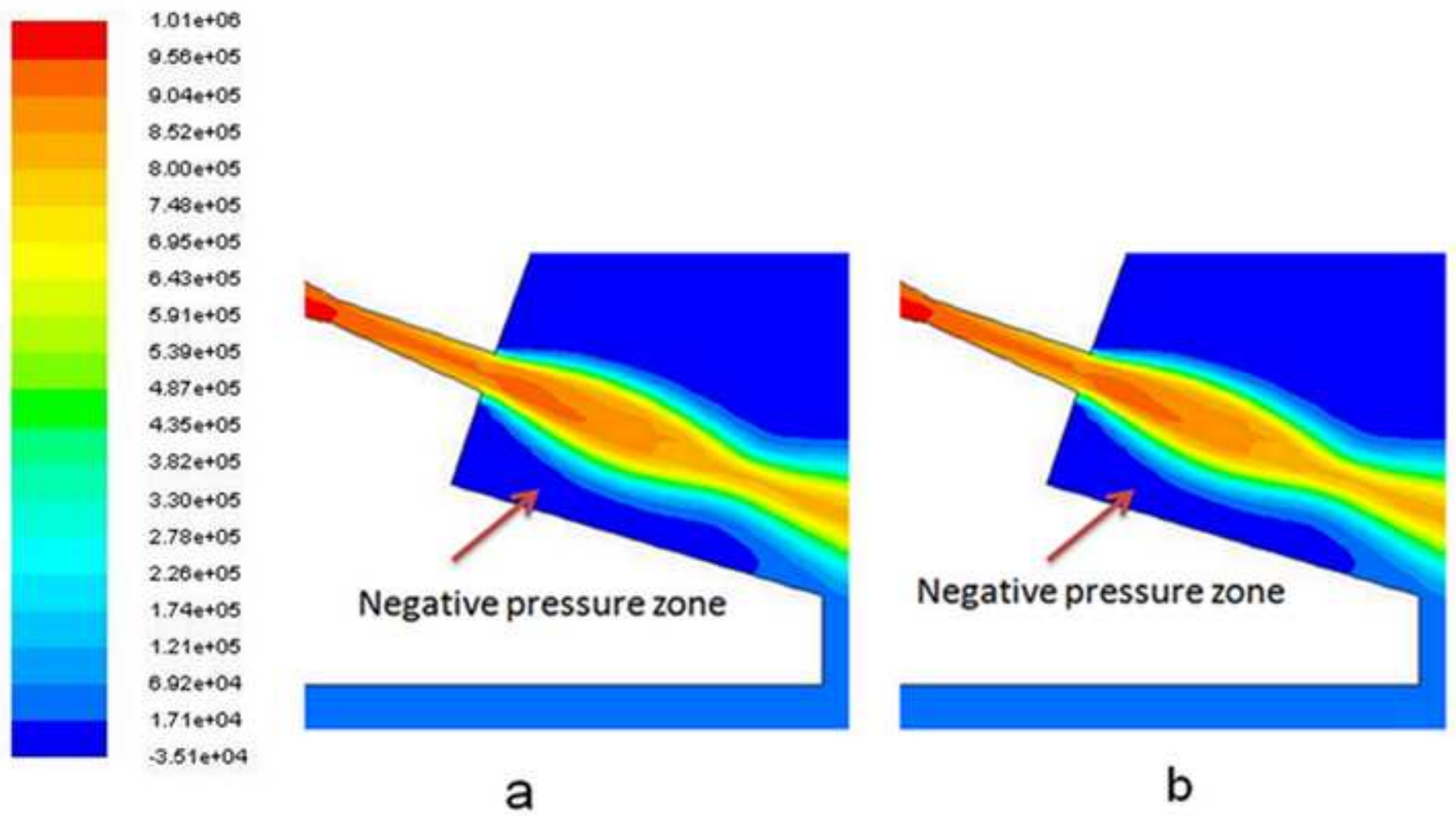
1.01e+06
9.56e+05
9.04e+05
8.52e+05
8.00e+05
7.48e+05
6.95e+05
6.43e+05
5.91e+05
5.39e+05
4.87e+05
4.35e+05
3.82e+05
3.30e+05
2.78e+05
2.26e+05
1.74e+05
1.21e+05
6.92e+04
1.71e+04
-3.51e+04
Negative pressure zone
Negative pressure zone
a
b

Figure 11

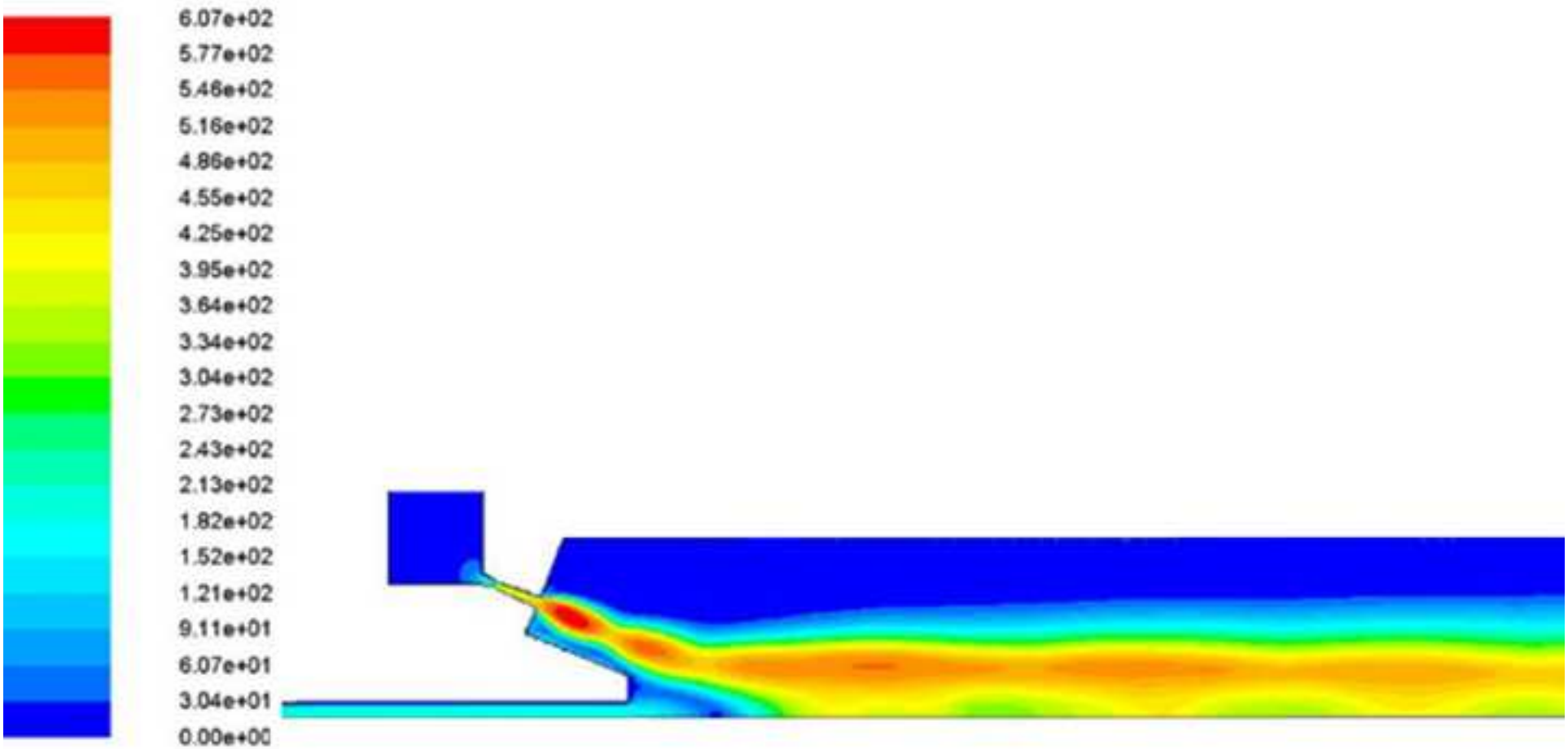
6.07e+02
5.77e+02
5.46e+02
5.16e+02
4.86e+02
4.55e+02
4.25e+02
3.95e+02
3.64e+02
3.34e+02
3.04e+02
2.73e+02
2.43e+02
2.13e+02
1.82e+02
1.52e+02
1.21e+02
9.11e+01
6.07e+01
3.04e+01
0.00e+00

Figure 12

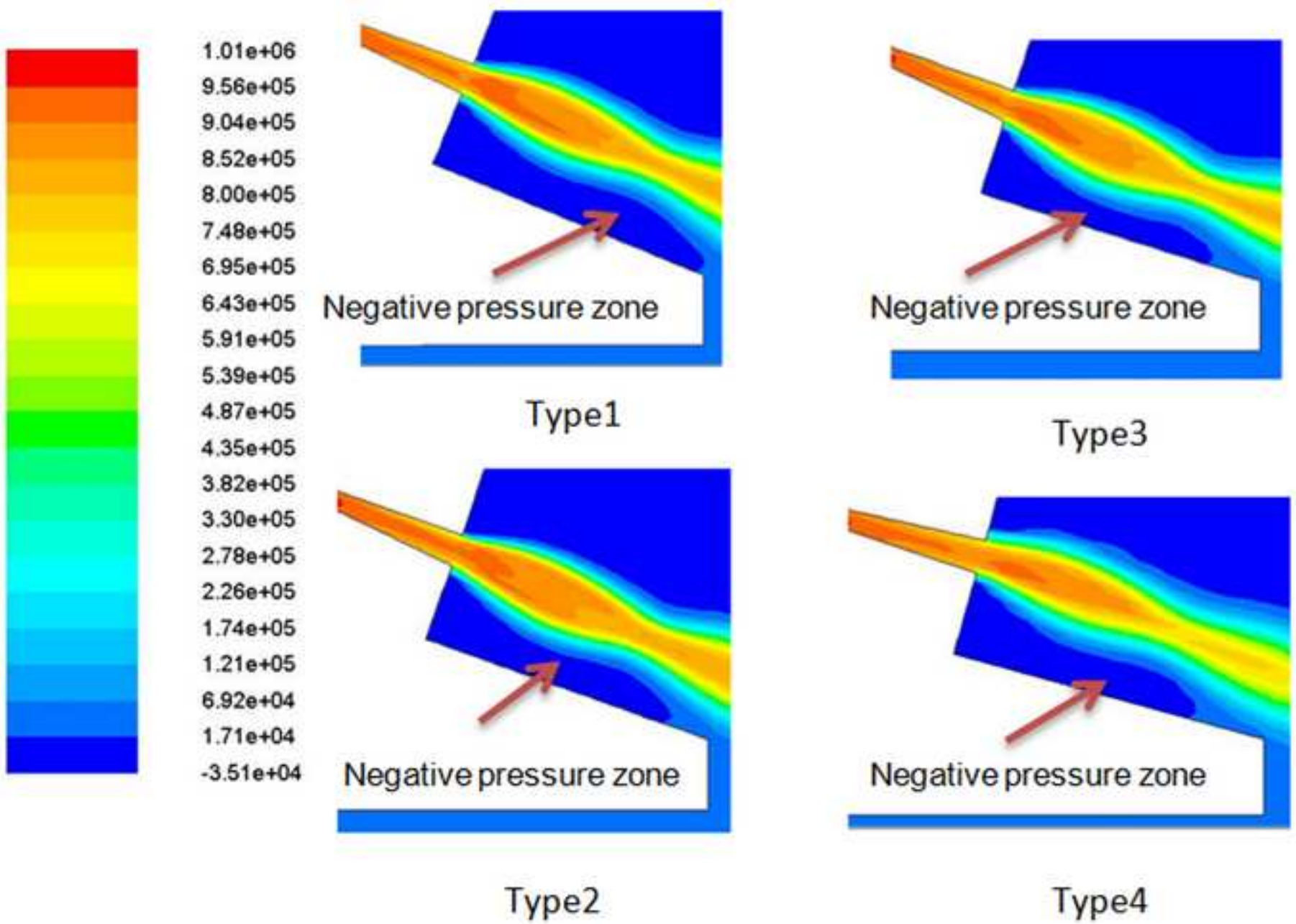
1.01e+06
9.56e+05
9.04e+05
8.52e+05
8.00e+05
7.48e+05
6.95e+05
6.43e+05
5.91e+05
5.39e+05
4.87e+05
4.35e+05
3.82e+05
3.30e+05
2.78e+05
2.26e+05
1.74e+05
1.21e+05
6.92e+04
1.71e+04
-3.51e+04
Negative pressure zone
Type1
Negative pressure zone
Type3
Negative pressure zone
Type2
Negative pressure zone
Type4

Figure 13

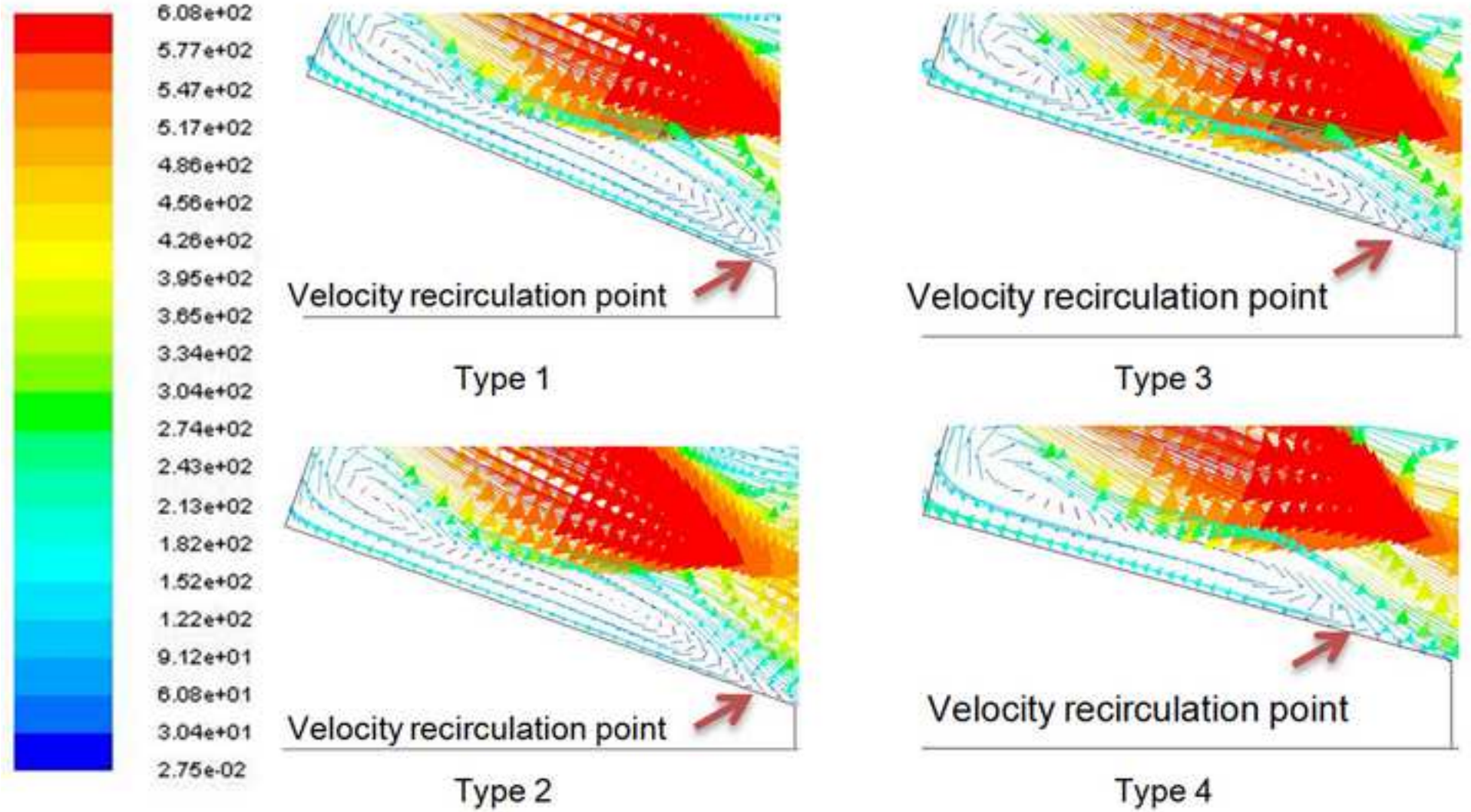
6.08e+02
5.77e+02
5.47e+02
5.17e+02
4.86e+02
4.56e+02
4.26e+02
3.95e+02
3.65e+02
3.34e+02
3.04e+02
2.74e+02
2.43e+02
2.13e+02
1.82e+02
1.52e+02
1.22e+02
9.12e+01
6.08e+01
3.04e+01
2.75e-02
Velocity recirculation point
Type 1
Velocity recirculation point
Type 3
Velocity recirculation point
Type 2
Velocity recirculation point
Type 4

Figure 14

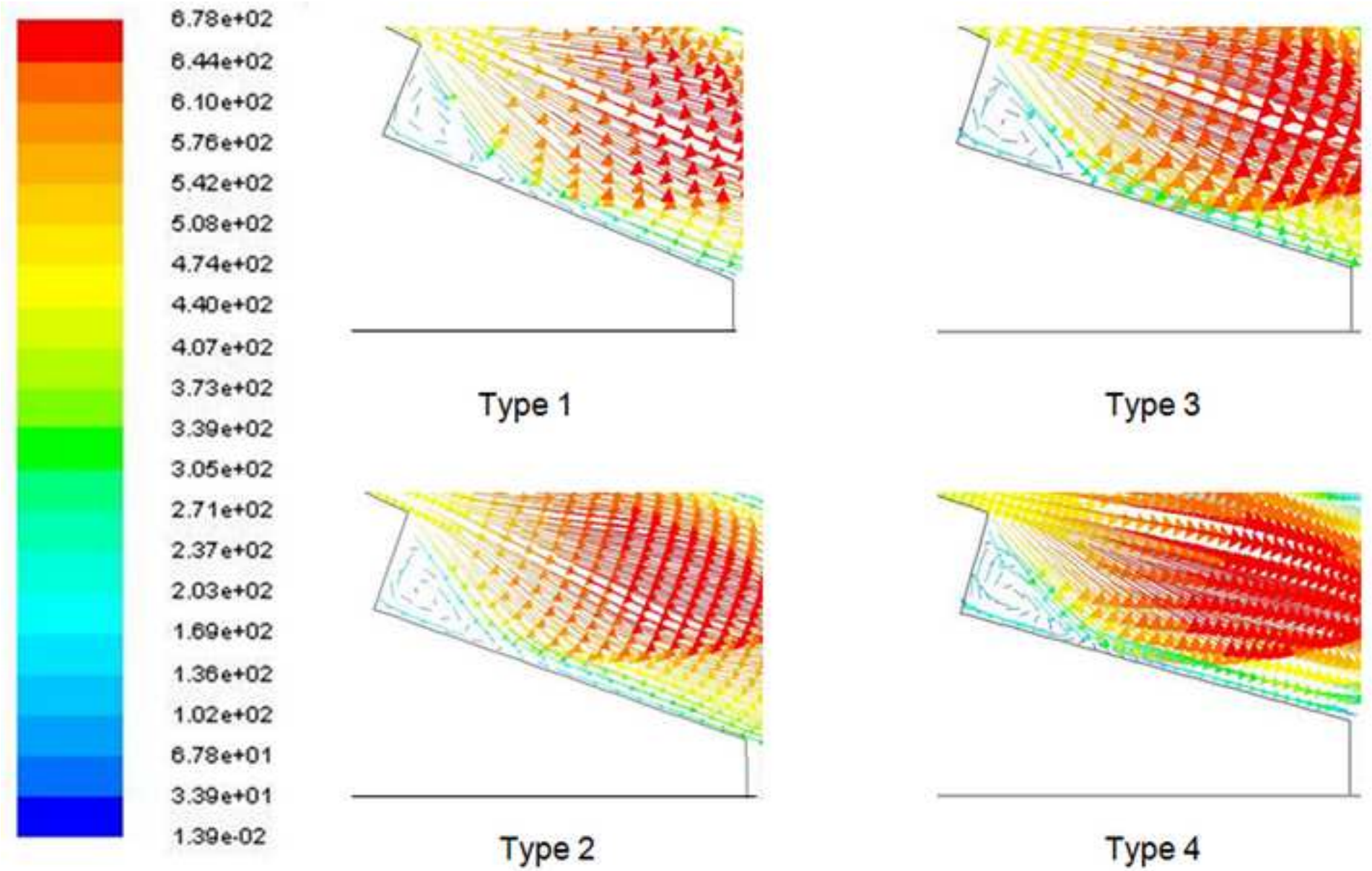
6.78e+02
6.44e+02
6.10e+02
5.76e+02
5.42e+02
5.08e+02
4.74e+02
4.40e+02
4.07e+02
3.73e+02
3.39e+02
3.05e+02
2.71e+02
2.37e+02
2.03e+02
1.69e+02
1.36e+02
1.02e+02
6.78e+01
3.39e+01
1.39e-02
Type 1
Type 3
Type 2
Type 4

Figure 15

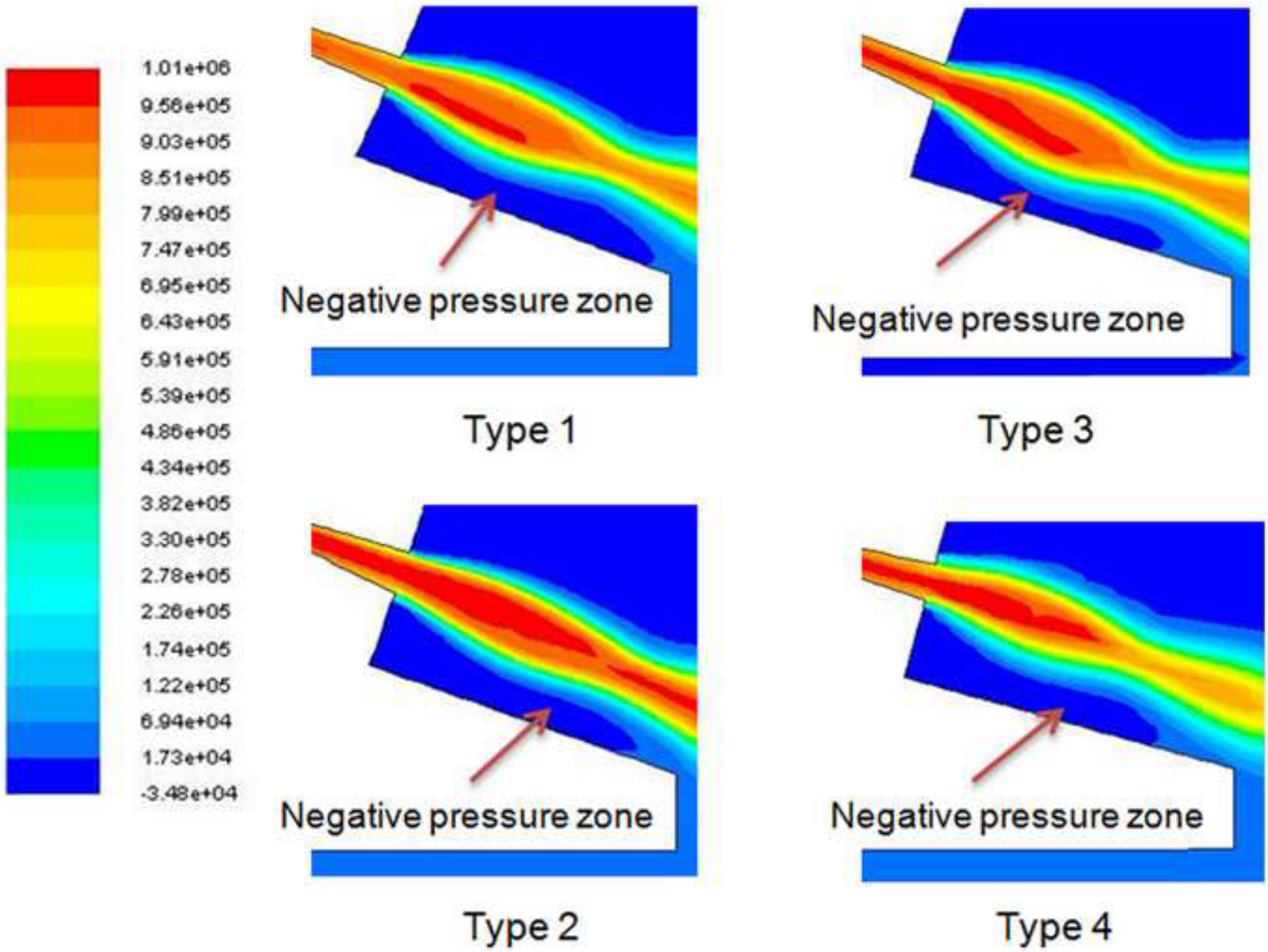
1.01e+06
9.56e+05
9.03e+05
8.51e+05
7.99e+05
7.47e+05
6.95e+05
6.43e+05
5.91e+05
5.39e+05
4.86e+05
4.34e+05
3.82e+05
3.30e+05
2.78e+05
2.26e+05
1.74e+05
1.22e+05
6.94e+04
1.73e+04
-3.48e+04
Negative pressure zone
Type 1
Negative pressure zone
Type 3
Negative pressure zone
Type 2
Negative pressure zone
Type 4